What is the most relevant soil structure parameter to describe field-measured N2O emissions?

Emile Maillet, Agnès Grossel, Isabelle Cousin, Laurent Arbaret, Lionel Cottenot, Marine Lacoste

Geoderma 453 (2025) 117155

Contents lists available at ScienceDirect

Geoderma

journal homepage: www.elsevier.com/locate/geoderma

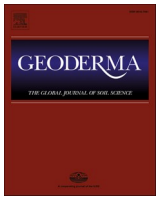

What is the most relevant soil structure parameter to describe field-measured N_2O emissions?

Emile Maillet [a], Agnès Grossel [a,*], Isabelle Cousin [a], Laurent Arbaret [b], Lionel Cottenot [a], Marine Lacoste [a]

[a] INRAE, Info&Sols, 45075, Orléans, France
[b] Université d'Orléans, CNRS/INSU, ISTO, UMR 7327, Orléans 45071, France

ARTICLE INFO

Handling Editor: D. Said-Pullicino

Keywords:
CT Scan
Greenhouse gas fluxes
Agricultural management
Gas transfer
Soil structure

ABSTRACT

Nitrous oxide (N_2O) emissions from soil are partly controlled by aeration and gas transfer in soil, and thus by soil structure. The intensity of N_2O emissions is usually expressed according to the water filled pore space (WFPS), calculated using the soil bulk density. These factors, even if they describe the soil structure and the water proportion in the porous network, do not inform about porous network characteristics among scales and their connectivity. The aim of this work was therefore to determine (1) to what extent the soil structure of an agricultural soil controlled N_2O emissions during a snap-shot campaign and (2) which metric of gas transfer or soil structure was the most appropriate to describe the N_2O emission variability at field scale. N_2O emissions were measured with a mobile chamber on a maize crop after fertilization with several soil management practices resulting in four soil states (strip-till versus tillage, compacted soil versus uncompacted) with contrasting soil structure. Soil cylinders and bulk soil were sampled from 24 plots exhibiting a strong gradient in N_2O emissions. Classical soil physical and chemical properties were measured, including soil bulk density and water filled pore space. Soil structure also was characterized quantitatively by X-ray tomography at meso and macro scales, and indirectly by gas transfer parameters. Clear differences were observed between low and high emission plots in terms of soil structure, soil temperature and nitrate concentration. However, soil structure appeared more strongly connected to N_2O emissions, and some thresholds on soil structural indicators were relevant to disentangle high and low N_2O fluxes. Some structural indicators at both scales (e.g. porosity, surface density) and gas transfer parameters (relative gas diffusivity, air permeability) were good descriptors of the observed N_2O fluxes. Nevertheless, the gas transfer parameters can be easily measured over a short period of time, whereas the soil structure indicators determined from 3D images require an acquisition and a processing phase that can be time consuming. A good compromise to evaluate the field N_2O flux potential from an easy measure would be to evaluate the relative gas diffusivity, which directly controls the diffusion of oxygen in soil and thereby the microbial processes of N_2O production.

1. Introduction

Due to its high warming potential, currently estimated to be equal to 273 the CO_2 warming potential (Li et al., 2024), nitrous oxide (N_2O) is considered as the third anthropogenic gas contributing to global warming (Ciais et al., 2014). Soils are a major source of N_2O emissions, which result from natural microbial processes, such as nitrification and denitrification (Butterbach-Bahl et al., 2013). Soil water and nitrogen contents, as well as soil temperature, are among the most influencing parameters to explain N_2O emissions (e.g. Conen et al., 2000). As far as water content is concerned, the highest N_2O emissions fluxes are usually observed for wet but unsaturated soils, at water-filled pore space (WFPS) lower than 90 % (Castellano et al., 2010; Davidson and Verchot, 2000). For such WFPS values, the gas diffusion is reduced, which limits the O_2 to be transported in the soil down to the microbial sites, and the anaerobiosis situation is in favor of N_2O production. The oxygen availability is actually considered as the highest influencing factor for nitrification and denitrification processes (Song et al., 2019). WFPS is used as a proxy of soil anoxia; its measurement is simple and it has been used in a massive amount of field N_2O studies.

* Corresponding author.
E-mail address: Agnes.grossel@inrae.fr (A. Grossel).

https://doi.org/10.1016/j.geoderma.2024.117155
Received 25 March 2024; Received in revised form 30 September 2024; Accepted 19 December 2024
Available online 28 December 2024

Several mechanisms govern the transport of gases in soil including O_2 and N_2O: gas transport by molecular diffusion (considered to be the predominant process) and gas transport by convection (Clough et al., 2005; Heincke & Kaupenjohann, 1999). The key variables characterizing these transfer processes are soil gas permeability for convection and soil gas diffusivity for diffusion, often normalized by air diffusivity, resulting in relative gas diffusivity. The work of B. C. Ball focused on the link between air permeability and N_2O emissions (Ball et al., 1997; Ball et al., 2008; Ball and Horgan, 2008; Ball, 2013). Several other studies explored the relationship between N_2O emissions and relative gas diffusivity (Balaine et al., 2013, 2016; Rousset et al., 2020, 2021). Relative gas diffusivity and air permeability control the level of soil oxygenation, and are then key properties of microbial activity (Martínez et al., 2016): high air permeability and relative gas diffusivity values make easier gas transfers in soils, whereas their low values favor anaerobiosis situations, which increase N_2O emissions (Ball, 2013). N_2O emissions would even increase in an exponential way when the relative gas diffusivity decreases down to a value of 0.005 (Balaine et al., 2016). The relative gas diffusivity should then be more adapted than the WFPS to explain N_2O emissions (Rohe et al., 2021).

Gas transfer in soils depends on soil structure, i.e. the three-dimensional arrangement of soil particles and aggregates (Dexter, 1988). This structure provides the biogeochemical interface which offers habitat for living species of different sizes (Rabot et al., 2014; Totsche et al., 2010), and regulates the soil functions (Vogel et al., 2022). The soil structure then strongly influences the Greenhouse Gas (GHG) emissions, which has been demonstrated for decades: Smith (1980) highlighted the role of interaggregate porosity, aggregates size and relative gas diffusivity, as control factors for anaerobiosis and denitrification. Whereas GHG production is of biological origin, Gregorich et al. (2006) also demonstrated that the physical soil quality controls N_2O emissions, due to its impact on physicochemical conditions responsible for biological activity. The description of the structure, especially pore-size distribution, connectivity of the porous network and saturation degree should be key elements to define N_2O emissions from the denitrification process (Ortega-Ramirez et al., 2023).

It was also shown that the localization of the particulate organic matter (POM) in the porosity, and more specifically the air-isolated volume of POM, was interesting to explain hotspots of N_2O emissions (Kravchenko et al., 2018; Ortega-Ramirez et al., 2023, Lucas et al., 2024). It seems for example that POM had higher water content than the bulk soil in relatively dry soil, allowing anoxic conditions and enhancement of the N_2O production (Kim et al., 2020, 2022; Kravchenko et al., 2017).

The scale at which soil structure is studied plays a crucial role in N_2O production and emission processes. Kravchenko et al. (2018) remind that biogeochemical processes involved in N_2O emissions occur in soil structure at several scales, from micron to millimeters. Kim et al. (2022) highlighted that, for a given WFPS, N_2O emissions would be higher in soils with large pore sizes (> 30 μm) than in fine pore sizes (< 10 μm), and Rabot et al. (2015) demonstrated that N_2O emissions peaks could be explained by reconnection of large pores during a rapid desiccation. 3D characterization of soil structure can be obtained from X Ray computed tomography (CT) scan (Rabot et al., 2018). The resolution of CT scan determines the studied scale for soil structure so several studies have dealt with the 3D characterisation of the soil structure at different scales (e.g. Houston et al., 2013; Lucas et al., 2020; Pot et al., 2020; Vogel et al., 2010). Some studies have linked 3D characterization of soil structure and N_2O production at the microscale (Lucas et al., 2023; Ortega-Ramírez et al., 2023; Rohe et al., 2021). As study scale is important, Lucas et al. (2024) used respectively CT scanning soil cylinders at 60 μm resolution and sub-samples at 19 μm to quantifiy oxygen and hotspots of aerobic respiration and POM. They found that both proximal and distal POM contribute to GHG emissions. CT scan is therefore a powerful tool to help theoretical understanding of denitrification hotspots leading to N_2O emissions by soils.

Nevertheless, previous studies were based on intact soil cores, which were incubated in controlled conditions in laboratory (e.g. Lucas et al., 2024; Ortega-Ramírez et al., 2023). Field N_2O emissions present a large variability linked to hotspot areas and soil structure is likely to explain part of this variability (van den Heuvel et al., 2009). The aim of the present work is to identify how the global characterization of soil structure at two scales, via the calculation of several structural indicators as well as the determination of POM, could help improve our understanding of direct field N_2O emissions from soils. N_2O emissions were then measured on an agricultural field where management practices have produced some contrasted soil structures in the surface horizon. At the locations with the highest and lowest emissions, soil physicochemical parameters were measured, and undisturbed soil cylinders were sampled, on which i) the gas transfer properties were measured and ii) the soil structure descriptors were determined from X-ray tomography images at 2 scales. The N_2O emissions, classical soil physical and chemical parameters (including WFPS and soil bulk density), gas transfer properties, and soil structure descriptors were interpreted together to identify the most relevant parameter to explain N_2O emissions.

2. Materials and methods

2.1. Study site

The studied agricultural field is a plot of 36 m wide and 60 m long located in a commercial farm, in the Loir river valley, approximately 120 km southwest of Paris (France), in the so-called OS^2 site ("Observatoire Orléanais Spatialisé des Sols") (Grossel et al., 2016; Gu et al., 2013). The climate records (1971–2000) in the closest meteorological station (Chartres, 48°270′N, 1°300′E, elevation 155 m a.s.l.) show a mean annual temperature of 10.6° C, with mean cumulative annual precipitation and potential evaporation of 598 mm and 740 mm, respectively. According to the IUSS Working Group WRB (2022), the soil of the study plot is a Ferric Luvisol, with a silty surface horizon (Table 1).

To analyze the effect of soil structure on N_2O emissions, we chose an agricultural plot experimenting different management practices, which intended to lead to several soil structural states. Following the maize harvest in October 2020, the plot was fully ploughed to a depth of 25 cm in December 2020 and left as bare soil until May 2021. Before the maize sowing (5th of May 2021), one half of the field (a strip of 18 m wide) was ploughed again at 25 cm depth, and the other half of the field was prepared using strip till, one of the non-inversion tillage practices used in conservation tillage systems (Morris et al., 2010). In the strip till zone each cultivated strip was separated by a 70 cm wide inter-row. The agricultural vehicle passed in the middle of each of the two 18 m plots, once during soil preparation (9,100 kg tractor with 2 bars pneumatic pressure) and a second time during sowing and fertilization (10,000 kg tractor with 1 bar pneumatic pressure). The field was then entirely

Table 1
Soil physico-chemical properties of the 24 selected plots (soil samples collected in the 0–7 cm depth of the topsoil horizon of the studied agricultural field).

Parameter	Minimum	Median	Maximum
Clay (0–0.002 mm, $g.kg^{-1}$)	147.0	178.5	203.0
Loam (0.002–0.05 mm, $g.kg^{-1}$)	763.0	778.5	812.0
Sand (0.05–2 mm, $g.kg^{-1}$)	34.0	42.5	49.0
C tot ($g.kg^{-1}$)	8.9	11.6	13.8
N tot ($g.kg^{-1}$)	1.1	1.3	1.6
C/N	8.0	8.6	9.6
pH	5.9	6.5	7.2
CEC (cmol + $.kg^{-1}$)	9.2	10.8	12.9
POM ($g.kg^{-1}$)	18.3	24.8	36.6
Bulk density ($g.cm^{-3}$)	1.2	1.4	1.5
WFPS (%)	50.9	64.6	75.3
Soil temperature (°C)	11.7	14.7	17.1
NO_3^- (mg $N.kg^{-1}$)	21.7	76.5	148.8

fertilized the 5th and 6th of May at 160 kg-N per hectare (solution composed by 50 % urea, 50 % ammonitrate).

The experimental measurements and the soil samplings were conducted under the two management practices (tillage and strip till), either under wheel tracks, or outside wheel tracks. Four soil structure conditions were then studied: i) "Compacted Tillage" (CT: zone on wheel tracks, that experimented tillage twice), ii) "Uncompacted Tillage" (UT: zone outside wheel tracks, that experimented tillage twice), iii) "Compacted Strip till" (CS: strip-tilled zone on wheel tracks), and iv) "Uncompacted Strip till" (US: strip-tilled zone outside wheel tracks).

2.2. N_2O emissions measurements

N_2O emissions were measured using a mobile chamber. The latter was coupled to a laboratory-built QCL spectrometer called SPIRIT with a laser wavelength of 4.5 μm and a sensitivity of 0.15 ppbv (at one standard deviation level) on N_2O analysis (Bureau et al., 2017; Guimbaud et al., 2011). The mobile chamber is directly pressed on the soil surface to ensure a quick N_2O emission measurement (Bureau et al., 2017; Grossel et al., 2014). For the present campaign a square mobile chamber of 23.5 cm side was chosen to allow sufficient room to sample the underlying soil for bulk and structural characterisation. N_2O accumulation was measured during 7 min. Some non-linearity of accumulation was observed at the beginning, due to the flux disturbance during the mobile chamber installation. So, the N_2O flux were calculated using a linear model after removal of the first minute of accumulation, following Cowan et al. (2014). The N_2O accumulation presents theoretically a non-linear shape because of the attenuation of the concentration gradient between soil and chamber atmosphere, and neglecting this effect can lead to an underestimation of N_2O emission, e.g. by up to 60 % in the study of Kroon et al. (2008). Moreover, using a mobile chamber without base insertion in soil and a linear fit can result in larger uncertainty in emission measurements. Nevertheless, these uncertainties are much smaller than the spatial variability which is always observed with the chamber measurements at field scale, generally of several orders of magnitude, and which was also observed on this study area (Grossel et al., 2014).

Emission measurements were performed on 20 different plots on each of the four studied soil states (CT, UT, CS, US) leading to a total of 80 N_2O measurements. Measurements were done on 18 and 19 May 2021 between 8:00 a.m. and 4:00p.m. in a randomly order. A stratified sampling was thereafter defined to select contrasted N_2O emissions plots for each soil state. Based on the N_2O emission distributions, three plots were randomly chosen in the first and in the fourth quartile of the N_2O emission distribution for each soil state. This resulted in six selected plots per soil state, leading to a total of 24 selected soil plots (Fig. 1).

The aim of the study is to identify hotspots and coldspots in the field and, immediately afterwards, collect soil samples at the precise locations where the N_2O measurements were taken. The goal is to figure out how physical and chemical properties could influence emission intensity, and in particular soil structural properties. In order to stratify our dataset according to the intensity of N_2O emissions, the 24 selected soil plots were classified in two N_2O emission categories, low vs. high emissions, using a threshold of 50 g-N ha^{-1} d^{-1}. To determine this threshold between low and high N_2O emissions, we looked at N_2O emissions in the OS^2 area over 15 years (INRAE database, not shown). Mean field emissions are observed between 5 and 10 g-N ha^{-1} d^{-1}. A value of 50 g-N ha^{-1} d^{-1} proved to be a very high N_2O flux value, even during N_2O emission peaks in spring when farmers were fertilizing. Among the 24 soil plots considered, we therefore assumed that soil plots exceeding a value of 50 g-N ha^{-1} d^{-1} were indeed hotspots.

All the N_2O fluxes selected in the upper quartile of N_2O emissions were larger than the chosen hotspot threshold of 50 g-N N_2O ha^{-1} d^{-1} for CS, US and CT soil state, but not for UT (Fig. 2). Therefore, all fluxes measured in the UT soil state were classified as low emission plots, resulting in $n = 15$ for low-emission plots and $n = 9$ for high-emission plots (Fig. 2). A statistical comparison using the Wilcoxon Mann-Whitney test was conducted to evaluate soil structural parameters, gas transfer parameters, and classical physical and chemical properties measured in low emission plots ($n = 15$) versus high emission plots ($n = 9$). After the identification of the 24 contrasted emissions plots, disturbed and undisturbed soil samples were collected on each plot to characterise the soil properties and the soil structure under the mobile chamber area. The soil temperature was also measured at each plot at 10 cm depth with a probe accurate to ± 0.1 °C (Hanna Instruments 4-Wire Pt100 Thermometer – HI955501).

2.3. Trade-off between number of soil samples and mobile chamber size

Studying the determinism of N_2O emissions requires the acquisition of many different variables, which in turn requires many different soil samples. Ideally, N_2O emissions should have been measured for each soil sample surface (bulk soil or soil cylinder), so that the N_2O measurement corresponded to the soil surface sampled. However, it is impossible to measure all the variables of interest on the same soil sample. This calls for a necessary compromise between:

- A large surface area investigated by the mobile chamber, implying a smoothing out of the spatial variability of N_2O fluxes, but on the other hand the possibility of taking numerous soil samples (bulk soil and soil cylinders) under the footprint of the mobile chamber. However, by proceeding in this way, it becomes less certain that the

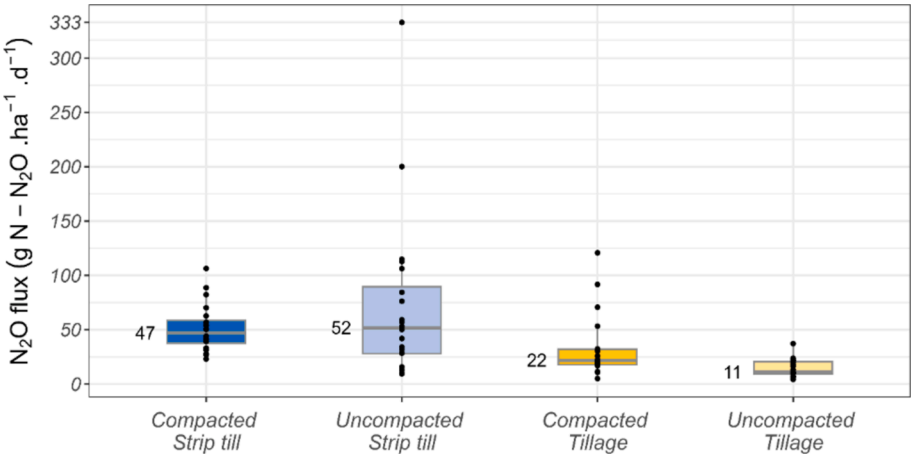

Fig. 1. N_2 O emissions measured for the four studied soil states. Measurements were done using a mobile chamber placed on 20 plots for each soil state.

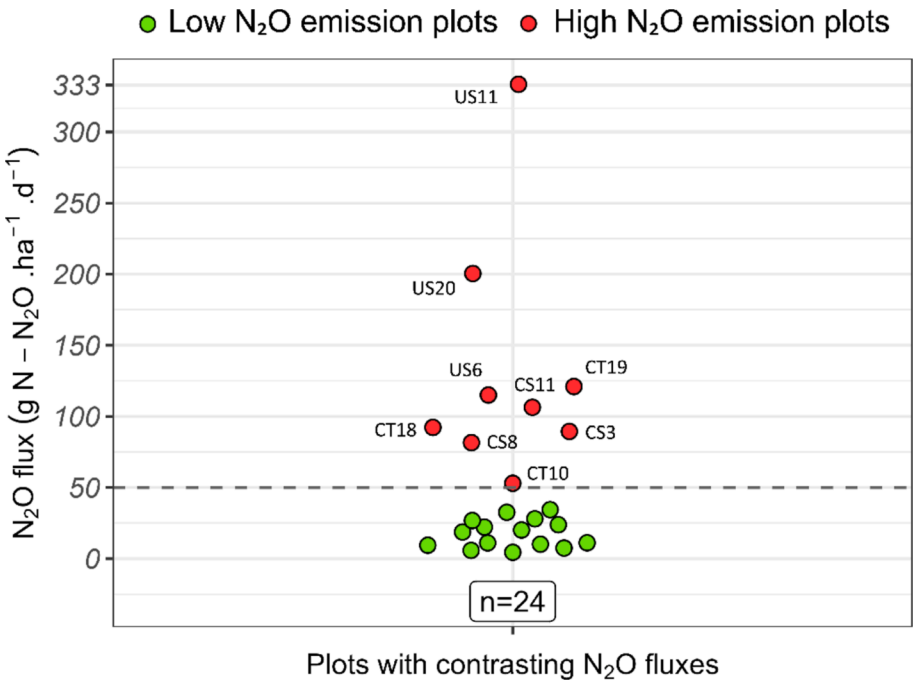

Fig.2. N_2 O emissions measured on the 24 selected soil plots; low (in green) vs. high (in red) emission plots (labels indicate plots identifiers; CT: compacted tillage, US: uncompacted strip till, CS: compacted strip till). (For interpretation of the references to color in this figure legend, the reader is referred to the web version of this article.)

results from bulk soil and soil cylinder analyses are representative of the measured N_2O flux.

- A small surface area investigated by the mobile chamber gives a detailed view of the spatial variability of N_2O fluxes, but also means that it is impossible to study several environmental variables at the same time.

We chose a mobile chamber surface large enough to sample both bulk soil and soil cylinders, in order to study the determinism of observed N_2O emissions as comprehensively as possible.

2.4. Characterisation of the soil properties and the soil structure

All the soil samples were collected on the 24 areas covered by the mobile chamber N_2O measurements.

2.4.1. Classical soil physical and chemical soil properties

On the 24 selected plots, bulk soil samples were collected in the surface horizon (0 to 7 cm depth). Before analyses, the soil was stored at 4 °C to limit biological activity. The gravimetric soil water content was measured from weighting soil at field humidity and after drying at 105 °C during 48 h. Soil aliquots were air dried at room temperature for about one month, crushed, sieved at 2 mm, and analyzed in the INRAE Soil Analysis Laboratory of (Arras, France). Soil organic carbon (SOC) and total N contents were analyzed by dry combustion at 1000 °C following the international standards (NF ISO 10694, 1995; NF ISO 13878, 1998). Soil clay, silt and sand contents were determined using the pipette method (NF X31-107, 2003), and pH was measured in water (1/5 v/v) (NF ISO 10390, 2005). Soil cation exchange capacity (CEC) was measured in cobalt hexamine trichloride (0.05 M) extract using spectrocolorimetry at 475 nm. The particulate organic matter (POM) content was the sum of the POM content in the 0–2 mm soil fraction (measured by the SADEF laboratory, France, NF ISO 14235), and the POM content in the soil fraction > 2 mm measured in the Info&Sols INRAE soil laboratory (Orléans, France).

Undisturbed soil samples were also collected to measure soil bulk density using soil cylinders of 260 cm^3 (71.5 mm internal diameter, 65 mm high; the same cylinders were first used to characterize the air permeability and the relative gas diffusivity, see section 2.3.2.) and following the national standard ISO 11272:2017. The WFPS was determined using the bulk density and water content values. The soil total porosity was estimated from the bulk density values using 2.65 g.cm^{-3} for the solid fraction density.

2.4.2. Characterisation of air permeability and relative gas diffusivity

Twenty-four undisturbed soil samples (cylinders of 71.5 mm internal diameter, 65 mm high) were collected on the selected soil plots, in the 0–7 cm soil top layer (stored for 15 months at 4 °C), and were then analysed at the Agroscope Laboratory (Zürich, Switzerland) to determine their air permeability and relative gas diffusivity. The air permeability was determined with a permeameter developed at Agroscope (Martínez et al., 2016), based on the steady state method proposed by Iversen et al. (2001). The soil cylinders were airtight-fixed to a steel cylinder connected to an airpipe. The airflow was recorded up to a stabilised flowrate at a pressure equal to 2 hPa. The air permeability was then calculated by using the Darcy's equation:

$$k_a = \frac{-Ql_s\eta}{\Delta_p A_s} \quad (1)$$

where Q is the volumetric flow rate ($m^3.s^{-1}$), l_s is the height of the soil sample (m), η is the dynamic air viscosity (Pa s), Δ_p is the difference in air pressure (Pa) and A_s is the cross-sectional area of the soil sample (m^2).

The effective gas diffusivity was measured on the same soil cylinder, by using a one-chamber apparatus developed by Agroscope (Martínez et al., 2016). It is based on the apparatus described by Schjønning et al. (2013), and used O_2 as the diffusing gas. From the measured effective gas diffusivity, the relative gas diffusivity was calculated:

$$D_r = \frac{D_p}{D_0} \quad (2)$$

where D_r is the relative gas diffusivity, D_p the measured gas diffusivity, and D_0 the gas diffusion coefficient of O_2 in air.

To link N_2O emissions measured in the field with gas transfer parameters, relative gas diffusivity and air permeability were measured at the soil water content of the field campaign. Gas transfer measurements are then as close as possible to the conditions under which N_2O fluxes are produced and emitted.

2.4.3. Characterisation of the soil structure at 2 scales: Computed tomography (CT) image acquisition

Another series of 24 undisturbed soil samples (cylinders of 24 mm internal diameter, 35 mm high) were collected on the selected soil plots, in the 0–7 cm soil top layer. They were stored for 15 months at 4 °C and then analyzed in the ISTO laboratory (Orleans, France) to characterize their structure at the mesoscale and macroscale levels (i.e., pore diameters greater than 30 μm, according to the classification by Cameron and Buchan, 2006). 3D images were obtained by using a Nanotom 180NF micro X-ray μ-CT device (GE Phoenix|x-ray, Wunstorf, Germany), with an operating voltage of 120 kV and a filament current of 35 to 45 μA (Al Majou et al., 2022). The scanning duration was about 3.5 h per soil sample. The resulting voxel size was of 15 x 15 x 15 μm.

A last series of 24 undisturbed soil samples (cylinders of 132 mm internal diameter, 70 mm high) were collected on the selected soil plots, in the 0–7 cm layer. They were stored for 2.5 months at 4 °C and were then analysed at the INRAE PIXANIM platform (Nouzilly, France) to characterise their structure at the macroscale level. 3D images were obtained by using a medical X-ray tomograph (Siemens Somatom Definition AS) operating at an energy level of 200 kV and a current of 140 mA (Rabot et al., 2015). The scanning duration was 75 s per soil sample. The voxel size was 291 x 291 x 100 mm.

2.5. Image processing

The workflow of the image processing and segmentation of the 3D soil images was adapted from Ortega-Ramirez et al. (2023), and most of the image processing was realized with the Fiji software (Schindelin et al., 2012). The images from the PIXANIM platform were first rescaled to obtain isotropic voxels of 290 μm. The image noise was reduced for all images (from the PIXANIM platform and ISTO laboratory) by using three successive filters: (i) a non local means filter to homogenize the different phases using the Biomedgroup plugin (Buades et al., 2011), with auto-estimation of the sigma and smoothing factors, (ii) an unsharp mask with a radius of 1 to enhanced edges (Schluter et al., 2014), and (iii) a median 3D filter with 2 by 2 by 2 voxels kernel to remove artefacts. All the images were then cropped to exclude non-soil areas based on previously defined regions of interest (ROI). The different soil phases were then separated using the Otsu global segmentation method (Otsu, 1979) through the Multi_OtsuThreshold plugin (Liao et al., 2001). Four thresholds were defined independently for each 3D images, allowing the identification of five soil phases: air, particulate organic matters (POM), a porous soil matrix, a dense soil matrix, and gravels. As recommended by Kravchenko et al. (2018); Kravchenko et al. (2014), the coherence of the thresholds allowing the POM detection was checked and manually adapted when necessary. Finally, a majority filter with a cubic kernel of 2 x 2 x 2 voxels was applied for the images ISTO laboratory using the C library QuantIm v.4 (Vogel, 2008), to remove very small elements which can be seen as noise. The two phases of soil matrix (porous and dense) were merged in the following image analysis.

2.6. Computation of morphological properties

Several soil structure indicators were computed using the 3D soil images to quantitatively characterize the soil structure. The volume of air-filled pores was estimated for the meso and macropores (later named as meso and macroporosity). The mesoporosity was calculated using the images from the ISTO laboratory at 15 μm resolution, selecting only the pores with a diameter between 30 μm and 75 μm. The macroporosity was calculated using the images from the PIXANIM platform at 290 μm resolution. This distinction between meso and macropores is based on the pore classification of Cameron and Buchan, 2006 (i.e. macropore diameter greater than 75 μm). The surface density, allowing the estimation of the exchange surface between the soil matrix and the air-filled porosity, was calculated for the meso and macroporosity using the QuantIm library (Vogel, 2008; Vogel et al., 2010). The Euler density, characterizing the connectivity of the air-filled pore space, was calculated for the whole porosity (meso and macroporosity) for the 3D images obtained at both resolutions (15 and 290 μm). It corresponds to the Euler number (Vogel et al., 2010) divided by the total volume of the considered soil (Koestel et al., 2020). A positive Euler density describes an unconnected pore network while a negative Euler number describes a connected pore network. The Euler density was calculated considering a neighborhood of 26 connected voxels with Fiji using the MorpholibJ plugin (Legland et al., 2016). Finally, the $Id_{\text{POM Air}}$ was calculated, also on the whole porosity (meso and macroporosity) for the 3D images obtained at both resolutions (15 and 290 μm). It was defined by Ortega-Ramirez et al. (2023) as the average value of the geodesic distances, i.e. the distance measured in the three-dimensional space, between the surface of each POM detected and the nearest air-filled pore. It was also determined with Fiji using the MorpholibJ plugin (Legland et al., 2016).

2.7. Data analysis

Untransformed N_2O flux data were analyzed using non-parametric statistics with a 5 % significance level, and the analyses were conducted using R software (R Core Team, 2022). The *wilcox.test()* function in the *stats* package was used for comparisons between statistic samples (Wilcoxon Mann Whitney test). Spearman's Rho values were obtained using the corrplot() function from the corrplot package (Wei and Simko, 2021) to assess the strength of relationships between variables. The *cor.mtest()* function from the *corrplot* package was also used, allowing only Rho with a p-value of less than 5 % to be shown in the Spearman matrix. Boxplots and scatterplots were produced using the *ggplot2* package (Wickham et al., 2016). False-color 3D images were produced using VGStudio MAX software.

3. Results

3.1. Measurements of N_2O emissions

N_2O emission measurements varied from 4 to 333 g-N ha^{-1} d^{-1} (Figs. 1 and 2). The distribution of the 80 measurements of N_2O emissions was lognormal (Shapiro-Wilk test on log-transformed fluxes, $p < 0.05$). This large variability is a well-known feature of N_2O emissions at the plot scale (Grossel et al., 2014).

3.2. Characterisation of the soil structure and associated parameters

3.2.1. Soil structure is strongly heterogeneous

From a qualitative point of view, a visual observation of the four soil states linked to the 4 management practices from the X-ray images at 2 scales shows contrasted soil structures (Fig. 3): the UT state presented the highest air-filled porosity, while the CS state exhibited have the poorest air-filled porosity, whatever the image resolution.

These differences in soil structure observed by a visual qualitative investigation are confirmed by the range of the soil calculated structural indicators (Table 2). The soil bulk density ranged from 1.21 $g.cm^{-3}$ to 1.49 $g.cm^{-3}$ and this indicator is consistent with the gas transfer properties, ranging from 1.4 to 104.7 μm^2 for air permeability and 0.003 to 0.077 for relative gas diffusivity. High variations were also observed for the soil macroporosity, which ranged from 0.2 to 10.4 %, and for the $Id_{\text{POM Air}}$ parameter calculated on 290 μm images which ranged from 575 to 9071 μm. The total porosity estimated through the bulk density values (ranging from 43.6 to 54.2 %) is much higher than the meso and macroporosity values estimated from the 3D soil images. This means

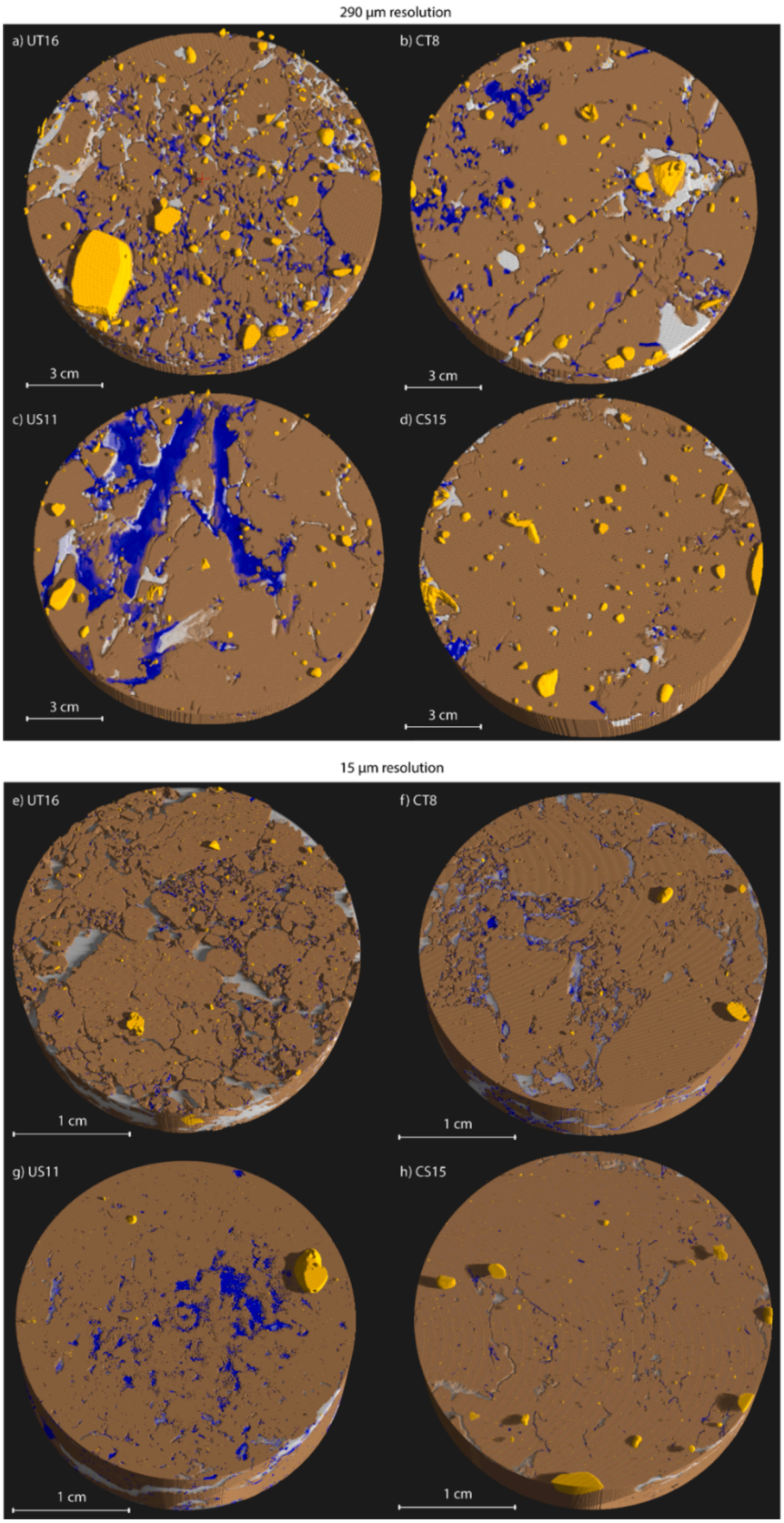

Fig. 3. Selected 2D cross-sections of segmented images for the four states (UT: uncompacted tillage, CT: compacted tillage, US: uncompacted strip till, CS: compacted strip till), showing in brown the soil matrix, in grey the air-filled porosity, in blue the POM and in yellow the gravels. The four upper cross-sections are from 290 µm resolution images (a, b, c and d), the four bottom cross-sections are from 15 µm resolution images (e, f, g, h). (For interpretation of the references to color in this figure legend, the reader is referred to the web version of this article.)

Table 2
Descriptive statistics of the soil structure indicators and the gas transfer properties.

Indicator (n = 24)	Minimum	Median	Maximum
Mesoporosity (%)	0.19	0.56	1.01
Macroporosity (%)	0.2	2.4	10.4
Surface density meso (m2.m^{-3})	0.15	0.45	0.83
Surface density macro (m2.m^{-3})	0.006	0.066	0.220
Euler density (15 μm; mm^{-3})	−0.18	1.40	2.50
Euler density (290 μm; mm^{-3})	0.0001	0.0007	0.0026
Id POM Air (15 μm; μm)	0.11	14	169
Id POM Air (290 μm; μm)	575	1447	9071
Bulk density (g.cm^{-3})	1.21	1.35	1.49
Total porosity (%)	43.6	48.9	54.2
Air permeability (μm^2)	1.4	13.5	104.7
Relative gas diffusivity	0.003	0.029	0.077

that the soil porosity with a diameter lower than the images resolution (undefined porosity) represents the major part of the total soil porosity.

3.2.2. *The scale used to characterise soil structure by CT scan has a strong influence on some structural indicators*

The surface density shows highest values for the mesoporosity than for the macroporosity (Table 2), which denotes a higher contact surface between the soil matrix and the air-filled porosity at the meso scale than as the macro scale. Only some air-filled pore networks observed on 15 μm resolution soil images were estimated to be connected (with negative Euler density), which means than potential porosity connectivity is mostly achieved with soil pores smaller than 15 μm. The soils of the selected plots had different POM contents (ranging from 18.3 to 36.6 g.kg^{-1}, Table 1); for the CT and UT states, POM are small fragments located within the inter-clods porosity (Fig. 3 a, b, e, f), while large fragments, probably crop residues incorporated into the soil, are visible in the 290 μm resolution images (Fig. 3 c). The $Id_{\text{POM Air}}$ shows the highest values when calculated on images with a resolution of 15 μm, rather than on images with a resolution of 290 μm (Table 2).

3.3. *Linking soil structure and N_2O emissions*

Regarding the Wilcoxon Mann-Whitney tests performed between low and high emission plots, a significant difference ($p < 0.05$) was observed between the two plot types for most of the studied soil properties known to influence N_2O emissions (10 of 14 studied properties; Fig. 4). Soils with high N_2O emissions showed significantly higher median values of WFPS, soil temperature, bulk density, and $Id_{\text{POM air}}$ (at the macroscale) than low-emission plots. These soils also had significantly lower median values for meso and macroporosity, meso and macro surface density, air permeability and relative gas diffusivity. Even if median differences were observed between the soils with high and low emissions for nitrate contents, Euler density (at the two scales) and $Id_{\text{POM Air}}$ (at the meso scale), these differences were not statistically significant. Other classical physico-chemical soil parameters, including laboratory measured POM content (g.kg^{-1}), did not allow significant difference (Wilcoxon Mann Whitney test) between low and high N_2O emission plots (Fig. S1).

The Spearman correlations between N_2O emissions measured in the field and all the analyzed factors were examined (detailed results can be found in supplementary material; Fig. S2). It demonstrates that the field N_2O emissions are negatively and more strongly related to relative gas diffusivity and to some structural indicators (like mesoporosity, macroporosity and surface density with $R \leq -0.6$) than other soil parameters classically used to explain N_2O emissions, such as WFPS, soil temperature and nitrate content, which are positively related. Euler density shows poorer correlation with N_2O emissions, and the nature of the relation is different regarding the considered scale ($R = 0.33$ at mesoscale, while $R = -0.47$ at macroscale). The POM content (g.kg^{-1}) also shows a poor Spearman correlation with N_2O emissions ($R = 0.3$).

4. Discussion: What are the most relevant parameters to evaluate N_2O emissions?

4.1. *What are the parameters likely to discriminate high and low N_2O emissions?*

The previous observations demonstrate that soil structure and gas transfer properties have a role in controlling the intensity of field measured N_2O fluxes, which is consistent with the known processes of N_2O emissions (Ball et al., 2013; Balaine et al., 2016). The soil physico-chemical and structural states observed in plots of high N_2O emissions are likely to favor a low partial pressure of oxygen in the soil atmosphere, compared with plots with low N_2O emissions:

- In plots with high emissions the median WFPS is around 73 % (Fig. 4. a), and WFPS ranging from 60 % to 90 % are known to lead to high N_2O fluxes (Balaine et al., 2013; Beare et al., 2009; Butterbach-Bahl et al., 2013; Davidson et al., 2000; Laville et al., 2011; Rabot et al., 2016; Ruser et al., 2006).
- Spearman correlation between soil temperature and N_2O emissions was weak ($R = 0.38$, Fig. 5), suggesting that temperature had a small effect on N_2O emissions. Slightly higher soil temperatures in the high-emission soil plots could potentially have stimulated aerobic respiration, thus accelerating oxygen consumption in isolated soil pores and ultimately promoting the expansion of anoxic microsites (Smith et al., 2003). Diurnal temperature variations are known to impact N_2O emissions but in the present campaign, however, hotspots were not linked to diurnal variations and were measured throughout the day (Fig. S3). The moderately higher soil temperature in hotspot areas could in fact be explained by the higher soil bulk density, as denser soils have higher thermal conductivity (Abu-Hamdeh and Reeder, 2000).
- In this study, nitrate concentration is high in all samples and is therefore not limiting for biochemical reactions producing N_2O (Table 1). It therefore seems normal not to have a strong Spearman correlation (Fig. S2) or a significant difference between plots with high and low soil emissions (Fig. 4).
- All the soils with high N_2O emissions have a relative gas diffusivity below 0.02. According to Stepniewski (1981), a relative gas diffusivity value between 0.005 and 0.02 indicates that the soil is anaerobic, which favors denitrification, often considered as the main microbial process leading to N_2O emissions (Scheer et al., 2020). Many authors have reported that denitrification begins at a relative gas diffusivity between 0.005–0.01 (Balaine et al. 2013; Chamindu Deepagoda et al. 2019; Li et al. 2021; Owens et al. 2017; Rousset et al. 2020), although values exceeding 0.02 have also been determined by Petersen et al. (2013) (work cited in Schlüter et al. 2024).
- A smaller pore volume at the meso and macroscale, with a smaller contact surface between the atmosphere and soil matrix, could enhance high N_2O emissions.

Other parameters, especially Euler Density and the $Id_{\text{POM Air}}$ seem to be irrelevant to discriminate between the high and low emissions.

As already mentioned, the mobile chamber used to measure N_2O fluxes in the field has a larger surface area than the soil cylinders scanned by CT-scan for the calculation of all structural indicators to enable measuring several soil parameters for the same N_2O flux measurement. The same is true for bulk soil samples collected to measure more classical physico-chemical parameters. This difference in size between the mobile chamber and the soil samples (bulk soil and soil cylinders) taken below is potentially the greatest source of unexplained variability. In addition, the potential reduction of N_2O to N_2 has not been quantified, adding to the uncertainty. In this context, very tight relationships between N_2O emissions and soil variables cannot be obtained, as often for field conditions, and correlation coefficients obtained for some variables can be considered as good.

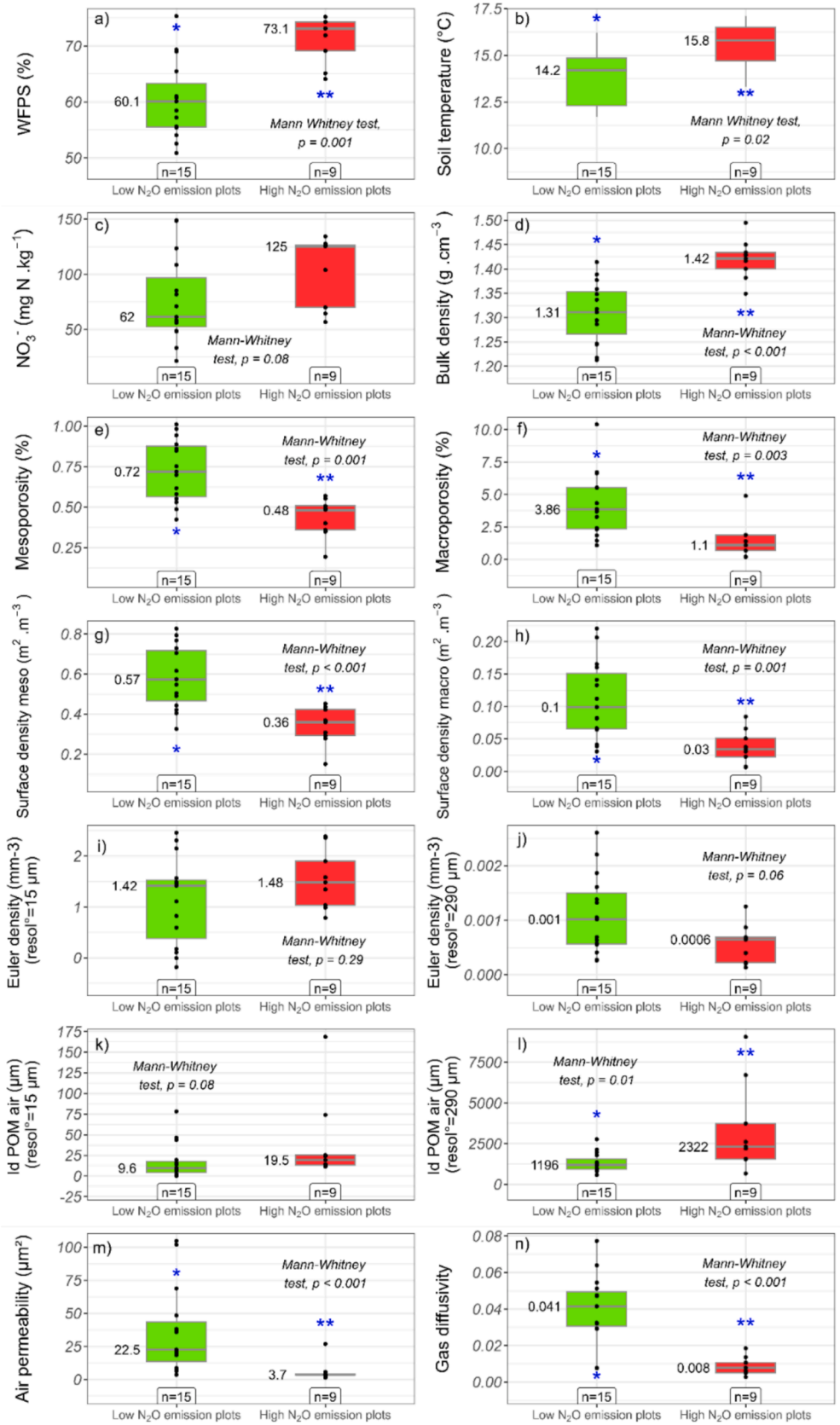

Fig. 4. Distribution of the soil parameters within the low emission plots (n = 15) and the high emissions plots (n = 9). A Mann-Whitney test was performed for each comparison. Different numbers of stars indicate statistical differences.

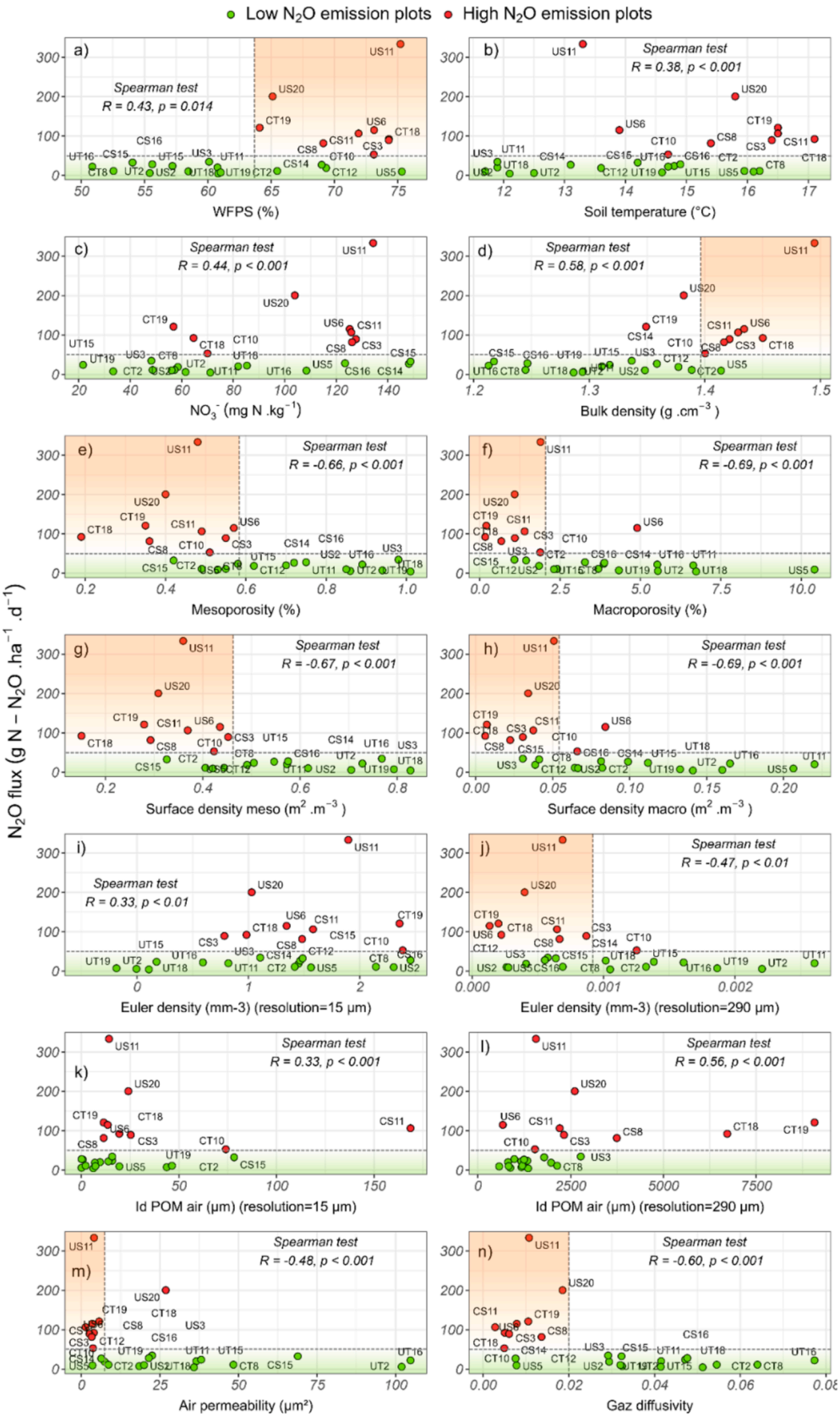

Fig. 5. Soil parameters as a function of N_2 O emissions. Low emissions are in green, high emissions in red. *UT: uncompacted tillage, CT: compacted tillage, US: uncompacted strip till, CS: compacted strip till. Horizontal dashed line: 50 g-N ha^{-1} d^{-1} , threshold separating low and high N_2 O emissions. Vertical dashed line: soil parameters threshold separating low and high N_2 O emissions.* (For interpretation of the references to color in this figure legend, the reader is referred to the web version of this article.)

4.2. Why are Euler density and $Id_{POM\ Air}$ irrelevant parameters in this study?

The calculation of the Euler density depends on the size of the smallest detectable pore, as a function of image resolution (Vogel et al., 2010). A finer resolution should theoretically result in a higher number of pores connected to each other (Lucas et al., 2019; Lucas et al., 2020), and then to more negative values. In this work, the Euler densities were always positive for most plots (all excepted one), indicating a disconnected pore network and not allowing this parameter to be used to discriminate between low and high N_2O emissions situations. Some studies have already evidenced a disconnected air porosity in 3D images with a coarse resolution. For example, Rabot et al. (2015) pointed out that the air-filled pore network is probably connected, but via pores of smaller size than those detected at the studied resolution (300 μm). The authors state that the total connectivity of the soil samples has thus been underestimated. Katuwal et al. (2015) suggest that Euler number is not a good metric for comparing macropore connectivity between soil samples. The authors also observed positive Euler number values from soils scanned at a resolution of 500 μm, synonymous of a disconnection of the pore network at the studied resolution. The Euler density should then be considered carefully for studying N_2O emission variability. Its value varies widely with the resolution of the image, and therefore with the scale of measurement chosen. It is consequently difficult to establish a relevant scale of measurement, and a compromise is necessary between the size of the considered soil sample and the pore sized targeted, that should be representative of the process of interest.

There are weak correlations between the POM content estimated from laboratory measurements ($g.kg^{-1}$) and image analysis at both 15 μm and 290 μm resolutions (Fig. S5), which may explain the weak correlation (Spearman test) between POM content ($g.kg^{-1}$) and N_2O emissions (Fig. S2 and S4). In contrast, the difference between $Id_{\ POM\ Air}$ values for low and high emission plots (Wilcoxon Mann Whitney test) was not significant for soil cylinders scanned at 15 μm (Fig. 4.k), but was significant for soil cylinders scanned at 290 μm (Fig. 4.l). The same trend was observed for the $Id_{\ POM\ Air}$ calculated both at 15 μm and 290 μm, i.e. the $Id_{\ POM\ Air}$ was higher in plots with high emissions than in plots with low emissions. It means that the Particulate Organic Matter within the hotspots is located at larger distances from the next air-filled pore than low-emission plots, which increases the likelihood of anoxic conditions in areas where C substrate is available for microbial processes. When the oxygen partial pressure becomes low or even zero, anaerobic microbial respiration can take place. The denitrification phenomenon is therefore likely to be favored within microbial hotspots, where nitrogen oxidants acting as alternative oxygen electron acceptors favor high production of N_2O. The latter is then transferred through the soil pore network to the atmosphere. Denitrification was likely the predominant process leading to the high N_2O emissions measured in this study, so the $Id_{\ POM\ Air}$ indicator should be relevant: the high emissions plots had actually higher $Id_{\ POM\ Air}$ values than the low emission plots, consistently with the previous findings of Ortega-Ramirez et al. (2023). The $Id_{\ POM\ Air}$ indicator brings another important information as it accounts for the effect of both structure and C substrate repartition in the soil porosity. However, it may be more difficult to use than some other structure indicators since a precise detection of POM is required, while thresholding POM in grey scale CT-scan images can be difficult (Baveye et al., 2018; Kravchenko et al., 2014). Indeed, the organic matter X-ray attenuation coefficients that generate grey levels between those of the soil matrix and air- or water-filled porosity (De Gryze et al., 2006; Peth et al., 2014), can lead to uncertainties.

4.3. Comparing WFPS and soil structure characteristics

WFPS is commonly used to assess the control of both soil structure and soil water content on N_2O emissions. In this study, a relation was also observed between WFPS and N_2O emissions, but not as strong as the relation between N_2O emissions and soil structure indicators, especially porosity and surface density (both at meso and macro scales) (Fig. 5). This may be because WFPS is calculated using soil bulk density, which does not consider how water and air are distributed in the pore space. As surface density is very strongly correlated with porosity (Spearman's test yielded R2 values of 0.97 at the macro scale and 0.99 at the meso scale, Fig. S2), it may be possible to calculate only one of the two indicators, although the two parameters do not provide the same information.

4.4. Comparing WFPS, gas transfer characteristics

Gas transfer parameters (especially relative gas diffusivity, and to a lesser extent air permeability) were also both good indicators of N_2O emission variability. Relative gas diffusivity presented a better relation with N_2O emissions than WFPS (R = -0.60, Spearman test, Fig. 5), which is consistent with the recommendations of some authors to analyze the relative gas diffusivity rather than the WFPS to study the N_2O emissions determinism. For example, Petersen et al. (2008) showed that the relative gas diffusivity explained the observed N_2O emissions better than the WFPS. In their study, Balaine et al. (2013) showed that the observed peak in N_2O emissions was poorly explained by WFPS, but strongly linearly correlated with relative gas diffusivity. Based on regression analyses, Balaine et al. (2016) also observed that relative gas diffusivity was better suited than WFPS to explain variations in N_2O concentration resulting from denitrification. Oxygen migration in the soil, expressed by relative gas diffusivity, would indeed be a better predictor than WFPS, because the parameter depends not only on the bulk density and water content of the soil (Balaine et al., 2013; Klefoth et al., 2014), but also on the connectivity and tortuosity of the air-filled pore space (Arthur et al., 2012; Rousset et al., 2022). Relative gas diffusivity is therefore highly integrative of the state of the soil structure at a given moment.

In this work, air permeability is negatively correlated with N_2O emissions with a lower correlation coefficient (in absolute value) ($R = -0.48$) than relative gas diffusivity ($R = -0.6$), which could be due to the fact that advection is not the main gas transfer process in the soil, due to the frequent low pressure gradients (Clough et al., 2005; Heincke and Kaupenjohann, 1999; Velthof et al., 1996). However, it is highly positively correlated with relative gas diffusivity (R = 0.82, Fig. S2). To evaluate N_2O emissions, it should theoretically be preferable to study the relative gas diffusivity because gas diffusion is the main transport mechanism in soils (Clough et al., 2005). However, measuring the air permeability of a soil cylinder is a very short process compared to the relative gas diffusivity measurement, lasting only a few minutes. If the gas relative diffusivity is a good descriptor of N_2O emissions and air permeability is highly correlated with the relative gas diffusivity, this makes air permeability a parameter also interesting to measure.

4.5. Comparing gas transfer properties and soil structure characteristics from 3D images

Mesoporosity and macroporosity are positively correlated with air permeability and gas relative diffusivity (Fig. S2), which is consistent with the fact that air porosity is a major component of gas transfer, as shown in previous studies (Balaine et al., 2016; Deepagoda et al., 2011; Katuwal et al., 2015; Kawamoto et al., 2006; Naveed et al., 2014; Rousset et al., 2020; Rousset et al., 2022). However, whereas soil structure indicators and gas transfer parameters require specific undisturbed samplings there is a strong difference in terms of measurements duration, because i) imagery needs more complex apparatus than gas transfer parameters and ii) calculating structural indicators using 3D imaging is time-consuming, compared to gas transfer parameters measurement.

4.6. Defining some threshold values for relevant parameters to evaluate N_2O emissions

The relations between N_2O emissions and the studied soil factors were explored (Fig. 5). To distinguish low and high N_2O emissions, threshold values were identified for some of the soil parameters that best explain the N_2O emissions: some structural parameters (meso and macroscale porosity, surface density, air permeability and relative gas diffusivity), as well as WFPS and bulk density. A threshold could also be defined for the Euler density at 290 μm resolution (e.g. at the macroscale), but not at 15 μm resolution (e.g. at the meso and the macroscale). No particular trends were observed in the relationship between N_2O fluxes measured in the field, and $Id_{\text{POM Air}}$ (regardless the considered resolution), soil temperature, nitrate concentration, Euler density at the mesoscale and macroscale. Additional results for other classical studied soil physico-chemical parameters can be found in supplementary material (Fig. S4).

Threshold values obtained for WFPS and relative gas diffusivity are 63 % and 0.02, consistently with previous studies (Balaine et al., 2016; Balaine et al., 2013). To our knowledge, no study proposed threshold values for porosity and surface density calculated at meso and macrostructure scales, for Euler density calculated at macrostructure scale, or for air permeability beyond which N_2O fluxes are high. For all the factors, the defined threshold values below which N_2O emissions are high have been summarised in a conceptual chart (Fig. 6). Two different soil profiles are described, to explain low and high emission spots.

5. Conclusion

In this work soils of high emission plots showed different physico-chemical and soil structure conditions compared to soil of low emissions plots. They had higher values of WFPS, soil temperature and nitrates, as well as a soil structure characterized by lower porosity, surface density and gas transfer capacity. This suggests that denitrification was the main N_2O production process, triggered by substrate availability as well as low aeration and gas transfer in soil. The WFPS still remains to be a relevant indicator to explain N_2O emissions. However, some structural indicators calculated by CT scan (porosity, surface density), as well as relative gas diffusivity and air permeability seem to be better in terms of information quality.

Nevertheless, regarding the structural indicators calculated by CT scan at two scales, consideration of a single scale could be sufficient, i.e. the macrostructure, as indicators calculated at the mesostructure scale did not provide more information. Among all the soil structure indicators studied, relative gas diffusivity appears to be the best soil structure parameter for describing N_2O emissions. Indeed, relative gas diffusivity is faster and easier to measure than 3D image-based indicators. It reflects not only soil water content but also pore volume, connectivity and tortuosity, influencing soil oxygen diffusion controlling denitrification and therefore N_2O emissions intensity.

Threshold values, below which high N_2O emissions have been observed, are proposed in this work. It would be interesting to verify and refine these thresholds in other pedoclimatic contexts, and for other agricultural practices.

CRediT authorship contribution statement

Emile Maillet: Writing – review & editing, Writing – original draft, Visualization, Methodology, Investigation, Formal analysis, Conceptualization. **Agnès Grossel:** Writing – review & editing, Writing – original draft, Supervision, Methodology, Investigation, Funding acquisition, Formal analysis, Data curation, Conceptualization. **Isabelle Cousin:** Writing – review & editing, Writing – original draft, Validation, Supervision, Methodology, Investigation, Funding acquisition, Data curation, Conceptualization. **Laurent Arbaret:** Writing – review & editing, Visualization, Software, Resources. **Lionel Cottenot:** Investigation, Validation, Writing – review & editing. **Marine Lacoste:** Writing – review & editing, Writing – original draft, Supervision, Software, Methodology, Investigation, Funding acquisition, Formal analysis, Data curation, Conceptualization.

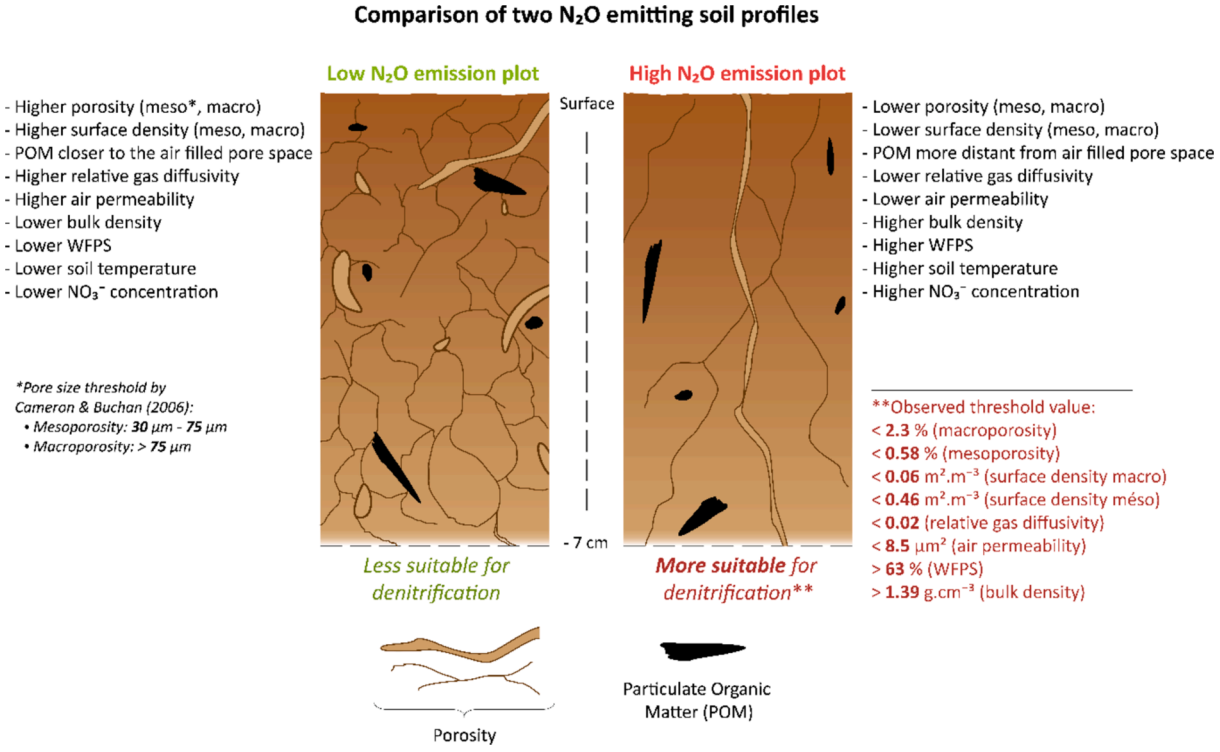

Fig. 6. Conceptual diagram describing the soil situations resulting in low or high N_2 O emissions, with the soil parameters thresholds values separating low and high N_2 O emissions (defined in this study).

Declaration of competing interest

The authors declare that they have no known competing financial interests or personal relationships that could have appeared to influence the work reported in this paper.

Acknowledgements

We gratefully thank Thomas Keller, Johannes Koestel and Marlies Sommer for their kind assistance in gas diffusivity and air permeability measurements at Agroscope, Zürich (Switzerland). We also gratefully acknowledge François Lecompte and Frédéric Elleboudt of the PIXANIM facility for their help to realize CT-scans at 290 μm and Philippe Penhoud for the CT-scans at 15 μm resolution at the IST O laboratory. This work was supported by the Centre Region and by the Labex Voltaire (ANR-10-LABX-100-01, France).

Appendix A. Supplementary data

Supplementary data to this article can be found online at https://doi.org/10.1016/j.geoderma.2024.117155.

Data availability

Data will be made available on request.

References

Abu-Hamdeh, N.H., Reeder, R.C., 2000. Soil Thermal Conductivity Effects of Density, Moisture, Salt Concentration, and Organic Matter. Soil Science Society of America Journal 64 (4), 1285–1290.

Al Majou, H., Bruand, A., Rozenbaum, O., Le Trong, E., 2022. Evaluation of the impact of freezing technique on pore-structure characteristics of highly decomposed peat using X-ray micro-computed tomography. International Agrophysics 36 (3), 223–233.

Arthur, E., Moldrup, P., Schjønning, P., Jonge, L.W., 2012. Linking Particle and Pore Size Distribution Parameters to Soil Gas Transport Properties. Soil Science Society of America Journal 76 (1), 18–27.

Balaine, N., Clough, T.J., Beare, M.H., Thomas, S.M., Meenken, E.D., Ross, J.G., 2013. Changes in relative gas diffusivity explain soil nitrous oxide flux dynamics. Soil Science Society of America Journal 77 (5), 1496–1505.

Balaine, N., Clough, T.J., Beare, M.H., Thomas, S.M., Meenken, E.D., 2016. Soil gas diffusivity controls N_2O and N_2 emissions and their ratio. Soil Science Society of America Journal 80 (3), 529–540.

Ball, B.C., 2013. Soil structure and greenhouse gas emissions: a synthesis of 20 years of experimentation. Eur. J. Soil Sci. 64 (3), 357–373.

Ball, B.C., Horgan, G.W., Clayton, H., Parker, J.P., 1997. Spatial variability of nitrous oxide fluxes and controlling soil and topographic properties. Journal of Environmental Quality 26 (5), 1399–1409. https://doi.org/10.2134/jeq1997.00472425002600050029x.

Ball, B.C., Horgan, G.W., Parker, J.P., 2008. Short-range spatial variation of nitrous oxide fluxes in relation to compaction and straw residues. European Journal of Soil Science 51 (4), 607–616. https://doi.org/10.1046/j.1365-2389.2000.00347.x.

Ball, C.I., Horgan, G., 2008. Dynamics of upward and downward N_2O and CO_2 fluxes in ploughed or no-tilled soils in relation to water-filled pore space, compaction and crop presence. Soil and Tillage Research 101 (1–2), 20–30. https://doi.org/10.1016/j.still.2008.05.012.

Baveye, P.C., Otten, W., Kravchenko, A., Balseiro-Romero, M., Beckers, E., Chalhoub, M., Darnault, C., Eickhorst, T., Garnier, P., Hapca, S., Kiranyaz, S., Monga, O., Mueller, C.W., Nunan, N., Pot, V., Schluter, S., Schmidt, H., Vogel, H.J., 2018. Emergent properties of microbial activity in heterogeneous soil microenvironments: different research approaches are slowly converging, yet major challenges remain. Frontiers in Microbiology 9, 48.

Beare, M.H., Gregorich, E.G., St-Georges, P., 2009. Compaction effects on CO_2 and N_2O production during drying and rewetting of soil. Soil Biol. Biochem. 41 (3), 611–621.

Buades, A., Coll, B., Morel, J.-M., 2011. Non-local means denoising. Image Processing on Line 1, 208–212.

Bureau, J., Grossel, A., Loubet, B., Laville, P., Massad, R., Haas, E., Butterbach-Bahl, K., Guimbaud, C., Hénault, C., 2017. Evaluation of new flux attribution methods for mapping N_2O emissions at the landscape scale. Agriculture, Ecosystems & Environment 247, 9–22.

Butterbach-Bahl, K., Baggs, E.M., Dannenmann, M., Kiese, R., Zechmeister-Boltenstern, S., 2013. Nitrous oxide emissions from soils: how well do we understand the processes and their controls? Philosophical Transactions of the Royal Society b: Biological Sciences 368 (1621), 20130122.

Cameron, K., Buchan, G., 2006. Porosity and pore size distribution. Encyclopedia of Soil Science 2, 1350–1353.

Castellano, M.J., Schmidt, J.P., Kaye, J.P., Walker, C., Graham, C.B., Lin, H., Dell, C.J., 2010. Hydrological and biogeochemical controls on the timing and magnitude of nitrous oxide flux across an agricultural landscape. Glob. Change Biol. 16 (10), 2711–2720.

Chamindu Deepagoda, T.K., Jayarathne, J.R.R.N., Clough, T.J., Thomas, S., Elberling, B., 2019. Soil-Gas Diffusivity and Soil-Moisture effects on N_2O Emissions from Intact Pasture Soils. Soil Science Society of America Journal 83 (4), 1032–1043. https://doi.org/10.2136/sssaj2018.10.0405.

Ciais, P., Sabine, C., Bala, G., et al., 2014. Carbon and other biogeochemical cycles. In: Climate Change 2013: the Physical Science Basis. Contribution of Working Group I to the Fifth Assessment Report of the Intergovernmental Panel on Climate Change Change. Cambridge University Press, pp. 465–570.

Clough, T.J., Sherlock, R.R., Rolston, D.E., 2005. A Review of the Movement and Fate of N2O in the Subsoil. Nutrient Cycling in Agroecosystems 72 (1), 3–11.

Conen, F., Dobbie, K.E., Smith, K.A., 2000. Predicting N_2O emissions from agricultural land through related soil parameters. Glob. Change Biol. 6 (4), 417–426.

Cowan, N., Famulari, D., Levy, P., Anderson, M., Reay, D., Skiba, U., 2014. Investigating uptake of N2O in agricultural soils using a high-precision dynamic chamber method. Atmospheric Measurement Techniques 7 (12), 4455–4462.

Davidson, E.A., Keller, M., Erickson, H.E., Verchot, L.V., Veldkamp, E., 2000. Testing a Conceptual Model of Soil Emissions of Nitrous and Nitric Oxides. BioScience 50 (8), 667.

Davidson, E.A., Verchot, L.V., 2000. Testing the hole-in-the-pipe model of nitric and nitrous oxide emissions from soils using the TRAGNET database. Glob. Biogeochem. Cycle 14 (4), 1035–1043.

De Gryze, S., Jassogne, L., Six, J., Bossuyt, H., Wevers, M., Merckx, R., 2006. Pore structure changes during decomposition of fresh residue: X-ray tomography analyses. Geoderma 134 (1–2), 82–96.

Deepagoda, T.K.K.C., Moldrup, P., Schjønning, P., de Jonge, L.W., Kawamoto, K., Komatsu, T., 2011. Density-Corrected Models for Gas Diffusivity and Air Permeability in Unsaturated Soil. Vadose Zone J. 10 (1), 226–238.

Dexter, A.R., 1988. Advances in characterization of soil structure. Soil and Tillage Research 11 (3–4), 199–238.

Gregorich, E., Rochette, P., Hopkins, D., Mckim, U., Stgeorges, P., 2006. Tillage-induced environmental conditions in soil and substrate limitation determine biogenic gas production. Soil Biology and Biochemistry 38 (9), 2614–2628.

Grossel, A., Nicoullaud, B., Bourennane, H., Rochette, P., Guimbaud, C., Chartier, M., Catoire, V., Henault, C., 2014. Simulating the spatial variability of nitrous oxide emission from cropped soils at the within-field scale using the NOE model. Ecol. Model. 288, 155–165.

Grossel, A., Nicoullaud, B., Bourennane, H., Lacoste, M., Guimbaud, C., Robert, C., Hénault, C., 2016. The effect of tile-drainage on nitrous oxide emissions from soils and drainage streams in a cropped landscape in Central France. Agriculture, Ecosystems & Environment 230, 251–260.

Gu, N.B., Rochette, P., Grossel, A., Hénault, C., Cellier, P., Richard, G., 2013. A regional experiment suggests that soil texture is a major control of N2O emissions from tile-drained winter wheat fields during the fertilization period. Soil Biology and Biochemistry 60, 134–141.

Guimbaud, C., Catoire, V., Gogo, S., Robert, C., Chartier, M., Laggoun-Défarge, F., Grossel, A., Albéric, P., Pomathiod, L., Nicoullaud, B., Richard, G., 2011. A portable infrared laser spectrometer for flux measurements of trace gases at the geosphere–atmosphere interface. Meas. Sci. Technol. 22 (7), 075601.

Heincke, M., Kaupenjohann, M., 1999. Effects of soil solution on the dynamics of N2O emissions: a review. 25.

Houston, A.N., Schmidt, S., Tarquis, A.M., Otten, W., Baveye, P.C., Hapca, S.M., 2013. Effect of scanning and image reconstruction settings in X-ray computed microtomography on quality and segmentation of 3D soil images. Geoderma 207–208, 154–165.

IUSS Working Group WRB. (2022). World Reference Base for Soil Resources. International soil classification system for naming soils and creating legends for soil maps. International Union of Soil Sciences (IUSS), 4th edition, Vienna, Austria. https://wrb.isric.org/documents/.

Iversen, B.V., Schjonning, P., Poulsen, T.G., Moldrup, P., 2001. In situ, on-site and laboratory measurements of soil air permeability: Boundary conditions and measurement scale. Soil Science 166 (2), 97–106.

Katuwal, S., Norgaard, T., Moldrup, P., Lamande, M., Wildenschild, D., de Jonge, L.W., 2015. Linking air and water transport in intact soils to macropore characteristics inferred from X-ray computed tomography. Geoderma 237, 9–20.

Kawamoto, K., Moldrup, P., Schjønning, P., Iversen, B.V., Komatsu, T., Rolston, D.E., 2006. Gas Transport Parameters in the Vadose Zone: Development and Tests of Power-Law Models for Air Permeability. Vadose Zone J. 5 (4), 1205–1215.

Kim, K., Guber, A., Rivers, M., Kravchenko, A., 2020. Contribution of decomposing plant roots to N_2O emissions by water absorption. Geoderma 375, 114506. https://doi.org/10.1016/j.geoderma.2020.114506.

Kim, K., Gil, J., Ostrom, N.E., Gandhi, H., Oerther, M.S., Kuzyakov, Y., Guber, A.K., Kravchenko, A.N., 2022. Soil pore architecture and rhizosphere legacy define N2O production in root detritusphere. Soil Biology and Biochemistry 166, 108565.

Klefoth, R.R., Clough, T.J., Oenema, O., Van Groenigen, J.-W., 2014. Soil Bulk Density and Moisture Content Influence Relative Gas Diffusivity and the Reduction of Nitrogen-15 Nitrous Oxide. Vadose Zone J. 13 (11), vzj2014.2007.0089.

Koestel, J., Larsbo, M., Jarvis, N., 2020. Scale and REV analyses for porosity and pore connectivity measures in undisturbed soil. Geoderma 366, 114206.

Kravchenko, A.N., Negassa, W., Guber, A.K., Schmidt, S., 2014. New Approach to Measure Soil Particulate Organic Matter in Intact Samples using X-Ray Computed Microtomography. Soil Science Society of America Journal 78 (4), 1177–1185.

Kravchenko, A.N., Toosi, E.R., Guber, A.K., Ostrom, N.E., Yu, J., Azeem, K., Rivers, M.L., Robertson, G.P., 2017. Hotspots of soil N2O emission enhanced through water absorption by plant residue. Nat. Geosci. 10 (7), 496-+.
Kravchenko, A.N., Guber, A.K., Quigley, M.Y., Koestel, J., Gandhi, H., Ostrom, N.E., 2018. X-ray computed tomography to predict soil N2O production via bacterial denitrification and N2O emission in contrasting bioenergy cropping systems. GCB Bioenergy 10 (11), 894–909.
Kroon, P.S., Hensen, A., Van Den Bulk, W.C.M., Jongejan, P.A.C., Vermeulen, A.T., 2008. The importance of reducing the systematic error due to non-linearity in N2O flux measurements by static chambers. Nutrient Cycling in Agroecosystems 82 (2), 175–186.
Laville, P., Lehuger, S., Loubet, B., Chaumartin, F., Cellier, P., 2011. Effect of management, climate and soil conditions on N2O and NO emissions from an arable crop rotation using high temporal resolution measurements. Agricultural and Forest Meteorology 151 (2), 228–240.
Legland, D., Arganda-Carreras, I., Andrey, P., 2016. MorphoLibJ : Integrated library and plugins for mathematical morphology with ImageJ. *Bioinformatics* 32 (22), 3532–3534.
Li, L.-J., Clough, T.J., Li, Y., Surey, R., Mueller, C.W., 2021. Contribution of Particulate and Mineral-Associated Organic Matter to Potential Denitrification of Agricultural Soils. Frontiers in Environmental Science 9, 12.
Li, Y., Tian, H., Yao, Y., Shi, H., Bian, Z., Shi, Y., Wang, S., Maavara, T., Lauerwald, R., Pan, S., 2024. Increased nitrous oxide emissions from global lakes and reservoirs since the pre-industrial era. Nat. Commun. 15 (1), 942.
Liao, P.-S., Chen, T.-S., Chung, P.-C., 2001. A fast algorithm for multilevel thresholding. J. Inf. Sci. Eng. 17 (5), 713–727.
Lucas, M., Schluter, S., Vogel, H.J., Vetterlein, D., 2019. Soil structure formation along an agricultural chronosequence. Geoderma 350, 61–72.
Lucas, M., Vetterlein, D., Vogel, H.J., Schluter, S., 2020. Revealing pore connectivity across scales and resolutions with X-ray CT. Eur. J. Soil Sci. 72 (2), 546–560.
Lucas, M., Gil, J., Robertson, G.P., Ostrom, N.E., Kravchenko, A., 2023. Changes in soil pore structure generated by the root systems of maize, sorghum and switchgrass affect in situ N_2O emissions and bacterial denitrification. Biology and Fertility of Soils. https://doi.org/10.1007/s00374-023-01761-1.
Lucas, M., Rohe, L., Apelt, B., Stange, C.F., Vogel, H.-J., Well, R., Schlüter, S., 2024. The distribution of particulate organic matter in the heterogeneous soil matrix—Balancing between aerobic respiration and denitrification. Science of the Total Environment 951, 175383. https://doi.org/10.1016/j.scitotenv.2024.175383.
Martínez, I., Chervet, A., Weisskopf, P., Sturny, W.G., Rek, J., Keller, T., 2016. Two decades of no-till in the Oberacker long-term field experiment: Part II. Soil porosity and gas transport parameters. Soil and Tillage Research 163, 130–140.
Morris, N.L., Miller, P.C.H., Orson, J.H., Froud-Williams, R.J., 2010. The adoption of non-inversion tillage systems in the United Kingdom and the agronomic impact on soil, crops and the environment-A review. Soil Tillage Res. 108 (1–2), 1–15.
Naveed, M., Moldrup, P., Vogel, H.J., Lamande, M., Wildenschild, D., Tuller, M., de Jonge, L.W., 2014. Impact of long-term fertilization practice on soil structure evolution. Geoderma 217, 181–189.
Ortega-Ramirez, P., Pot, V., Laville, P., Schluter, S., Amor-Quiroz, D.A., Hadjar, D., Mazurier, A., Lacoste, M., Caurel, C., Pouteau, V., Chenu, C., Basile-Doelsch, I., Henault, C., Garnier, P., 2023. Pore distances of particulate organic matter predict N2O emissions from intact soil at moist conditions. Geoderma 429.
Otsu, N., 1979. A Threshold Selection Method from Gray-Level Histograms. IEEE Transactions on Systems, Man, and Cybernetics 9 (1), 62–66.
Owens, J., Clough, T.J., Laubach, J., Hunt, J.E., Venterea, R.T., 2017. Nitrous Oxide Fluxes and Soil Oxygen Dynamics of Soil Treated with Cow Urine. Soil Science Society of America Journal 81 (2), 289–298. https://doi.org/10.2136/sssaj2016.09.0277.
Petersen, S.O., Ambus, P., Elsgaard, L., Schjønning, P., Olesen, J.E., 2013. Long-term effects of cropping system on N_2O emission potential. Soil Biology and Biochemistry 57, 706–712. https://doi.org/10.1016/j.soilbio.2012.08.032.
Petersen, S., Schjonning, P., Thomsen, I., Christensen, B., 2008. Nitrous oxide evolution from structurally intact soil as influenced by tillage and soil water content. Soil Biology and Biochemistry 40 (4), 967–977.
Peth, S., Chenu, C., Leblond, N., Mordhorst, A., Garnier, P., Nunan, N., Pot, V., Ogurreck, M., Beckmann, F., 2014. Localization of soil organic matter in soil aggregates using synchrotron-based X-ray microtomography. Soil Biol. Biochem. 78, 189–194.
Pot, V., Zhong, X., Baveye, P.C., 2020. Effect of resolution, reconstruction settings, and segmentation methods on the numerical calculation of saturated soil hydraulic conductivity from 3D computed tomography images. Geoderma 362, 12.
R Core Team, 2022. R: A Language and Environment for Statistical Computing. R Foundation for Statistical Computing, Vienna.
Rabot, E., Henault, C., Cousin, I., 2014. Temporal variability of nitrous oxide emissions by soils as affected by hydric history. Soil Science Society of America Journal 78 (2), 434–444.
Rabot, E., Lacoste, M., Hénault, C., Cousin, I., 2015. Using X-ray computed tomography to describe the dynamics of nitrous oxide emissions during soil drying. Vadose Zone J. 14 (8).
Rabot, E., Henault, C., Cousin, I., 2016. Effect of the soil water dynamics on nitrous oxide emissions. Geoderma 280, 38–46.
Rabot, E., Wiesmeier, M., Schlüter, S., Vogel, H.-J., 2018. Soil structure as an indicator of soil functions: A review. Geoderma 314, 122–137. https://doi.org/10.1016/j.geoderma.2017.11.009.
Rohe, L., Apelt, B., Vogel, H.-J., Well, R., Wu, G.-M., Schlüter, S., 2021. Denitrification in soil as a function of oxygen availability at the microscale. Biogeosciences 18 (3), 1185–1201.
Rousset, C., Clough, T.J., Grace, P.R., Rowlings, D.W., Scheer, C., 2020. Soil type, bulk density and drainage effects on relative gas diffusivity and N2O emissions. Soil Research 58 (8), 726.
Rousset, C., Clough, T.J., Grace, P.R., Rowlings, D.W., Scheer, C., 2021. Irrigation scheduling with soil gas diffusivity as a decision tool to mitigate N_2O emissions from a urine-affected pasture. Agriculture 11 (5), 443. https://doi.org/10.3390/agriculture11050443.
Rousset, C., Clough, T.J., Grace, P.R., Rowlings, D.W., Scheer, C., 2022. Wetting and drainage cycles in two New Zealand soil types: Effects on relative gas diffusivity and N2O emissions. Geoderma Regional 29, e00504.
Ruser, R., Flessa, H., Russow, R., Schmidt, G., Buegger, F., Munch, J.C., 2006. Emission of N_2O, N_2 and CO_2 from soil fertilized with nitrate: Effect of compaction, soil moisture and rewetting. Soil Biol. Biochem. 38 (2), 263–274.
Scheer, C., Fuchs, K., Pelster, D.E., Butterbach-Bahl, K., 2020. Estimating global terrestrial denitrification from measured N_2O:(N_2O + N_2) product ratios. Current Opinion in Environmental Sustainability 47, 72–80.
Schindelin, J., Arganda-Carreras, I., Frise, E., Kaynig, V., Longair, M., Pietzsch, T., Preibisch, S., Rueden, C., Saalfeld, S., Schmid, B., Tinevez, J.Y., White, D.J., Hartenstein, V., Eliceiri, K., Tomancak, P., Cardona, A., 2012. Fiji: an open-source platform for biological-image analysis. Nature Methods 9 (7), 676–682.
Schjønning, P., Eden, M., Moldrup, P., De Jonge, L.W., 2013. Two-chamber, two-gas and one-chamber, one-gas methods for measuring the soil-gas diffusion coefficient: validation and inter-calibration. Soil Science Society of America Journal 77 (3), 729–740.
Schlüter, S., Lucas, M., Grosz, B., Ippisch, O., Zawallich, J., He, H., Dechow, R., Kraus, D., Blagodatsky, S., Senbayram, M., Kravchenko, A., Vogel, H.-J., Well, R., 2024. The anaerobic soil volume as a controlling factor of denitrification: A review. Biology and Fertility of Soils. https://doi.org/10.1007/s00374-024-01819-8.
Schluter, S., Sheppard, A., Brown, K., Wildenschild, D., 2014. Image processing of multiphase images obtained via X- ray microtomography: A review. Water Resour. Res. 50 (4), 3615–3639.
Smith, K.A., 1980. A model of the extent of anaerobic zones in aggregated soils, and its potential application to estimates of denitrification. Journal of Soil Science 31 (2), 263–277.
Smith, K.A., Ball, T., Conen, F., Dobbie, K.E., Massheder, J., Rey, A., 2003. Exchange of greenhouse gases between soil and atmosphere: interactions of soil physical factors and biological processes. Eur. J. Soil Sci. 54 (4), 779–791.
Song, X., Ju, X., Topp, C.F.E., Rees, R.M., 2019. Oxygen regulates nitrous oxide production directly in agricultural soils. Environmental Science & Technology 53 (21), 12539–12547.
Stepniewski, W., 1981. Oxygen-diffusion and strength as related to soil compaction. II. Oxygen diffusion coefficient. Polish Journal of Soil Science 14 (1), 3–13.
Totsche, K.U., Rennert, T., Gerzabek, M.H., Kögel-Knabner, I., Smalla, K., Spiteller, M., Vogel, H.J., 2010. Biogeochemical interfaces in soil: The interdisciplinary challenge for soil science. Journal of Plant Nutrition and Soil Science 173 (1), 88–99.
van den Heuvel, R.N., Hefting, M.M., Tan, N.C.G., Jetten, M.S.M., Verhoeven, J.T.A., 2009. N_2O emission hotspots at different spatial scales and governing factors for small scale hotspots. Science of the Total Environment 407 (7), 2325–2332. https://doi.org/10.1016/j.scitotenv.2008.11.010.
Velthof, G.L., Jarvis, S.C., Stein, A., Allen, A.G., Oenema, O., 1996. Spatial variability of nitrous oxide fluxes in mown and grazed grasslands on a poorly drained clay soil. Soil Biology and Biochemistry 28 (9), 1215–1225.
Vogel, H.J., 2008. QuantIm: C/C++ library for scientific image processing. Helmholtz Ctr. for Environ. Res, Halle, Germany.
Vogel, H.J., Weller, U., Schlüter, S., 2010. Quantification of soil structure based on Minkowski functions. Computers & Geosciences 36 (10), 1236–1245.
Vogel, H.J., Balseiro-Romero, M., Kravchenko, A., Otten, W., Pot, V., Schluter, S., Weller, U., Baveye, P.C., 2022. A holistic perspective on soil architecture is needed as a key to soil functions. Eur. J. Soil Sci. 73 (1), 14.
Wei, T., Simko, V., 2021. R package 'corrplot' : Visualization of a Correlation Matrix (Version 0.92). https://github.com/taiyun/corrplot.
Wickham, H., Chang, W., Wickham, M.H., 2016. Package 'ggplot2'. Create elegant data visualisations using the grammar of graphics. Version 2 (1). https://ggplot2.tidyverse.org.